

Doctoral Thesis

Human Dosimetry and Compliance
Assessment for Low Frequency
Magnetic Field Exposure
(低周波磁界ばく露に対する
ドシメトリと適合性評価)

January 2022

Keishi Miwa

Contents

<i>Contents</i>	<i>i</i>
<i>List of Figures.....</i>	<i>iii</i>
<i>List of Tables.....</i>	<i>v</i>
Chapter 1 Introduction	1
1.1. Background.....	1
1.1.1. International Guidelines and Standards for Human to Electromagnetic Field Exposure	1
1.1.2. Compliance Assessment Standard.....	3
1.1.3. Review of Previous Studies and Research Necessity.....	5
1.2. Contents of Thesis	7
Chapter 2 Models and Methods.....	9
2.1. Overview.....	9
2.2. Numerical Human Body Model	10
2.2.1. Cuboid and Ellipsoidal Model.....	10
2.2.2. Anatomical Model.....	11
2.3. WPT System.....	12
2.3.1. Schematic Diagram of WPT System.....	12
2.3.2. WPT Coil.....	13
2.4. Computational Methods	14
2.4.1. Induced Electric Field.....	14
2.4.2. Post-processing Algorithm	15
2.4.3. Coupling Factor.....	16
Chapter 3 A Method for Predicting the Induced Electric Field for Local Exposure....	18
3.1. Overview.....	18

3.2.	Exposure Scenario	19
3.3.	Results.....	19
3.3.1.	Derivation of Empirical Formula	19
3.3.2.	Comparison Between Formula and SPFD & FEM for Cuboid Model	23
3.3.3.	Effect of Model Shape.....	25
3.3.4.	Effect of Tissue Inhomogeneity	30
3.4.	Discussion & Conclusion.....	31
<i>Chapter 4 Compliance Assessment for Wireless Power Transfer Systems in Vehicle for Local and Nonuniform Exposure</i>		<i>34</i>
4.1.	Overview.....	34
4.2.	Exposure Scenario	35
4.3.	Results.....	36
4.3.1.	Distribution of Magnetic Field	36
4.3.2.	Induced Electric Field in Human Body	38
4.3.3.	Coupling Factor	40
4.4.	Discussion & Conclusion.....	41
<i>Chapter 5 Effects of Skin-to-Skin Contact for Post-processing Algorithm.....</i>		<i>43</i>
5.1.	Overview.....	43
5.2.	Exposure Scenario	44p
5.3.	Results.....	44
5.3.1.	Induced Electric Field.....	44
5.3.2.	Coupling Factor	48
5.4.	Discussion and Conclusion	49
<i>Chapter 6 Summary.....</i>		<i>50</i>
<i>Acknowledgements</i>		<i>53</i>
<i>References.....</i>		<i>54</i>

List of Figures

Figure 1.1 Assessment procedure for low frequency exposure.....	4
Figure 2.1 Schematic explanation of model: (a) cuboid model, (b) tissue composition of cuboid model and ellipsoidal model.....	10
Figure 2.2 Schematics of anatomical human body model: (a) whole body, (b) head and trunk, (c) arm and (d) leg.....	11
Figure 2.3 Schematic diagram of WPT vehicle.....	12
Figure 2.4 Schematic diagram of WPT coils: (a) transmitting and (b) receiving coils.....	13
Figure 3.1 Distribution of (a) scalar potential and (b) electric field electric field computed using the SPFD method; $\alpha = 0.4$ m, $\gamma = 1.2$ m. and $\gamma = 1.2$ m.	20
Figure 3.2 Normalized scalar potentials on the long edge of the cuboid model for (a) $\gamma = 0.4$ m, (b) $\gamma = 0.8$ m, (c) $\gamma = 1.2$ m, and (d) $\gamma = 1.6$ m. $\alpha = 0.4$ m.	21
Figure 3.3 Distribution for cuboid with $\alpha = \gamma = 0.4$ m (SPFD); (a) IEF and (b) scalar potential.	23
Figure 3.4 Distribution of (a) scalar potential and (b) IEF in ellipsoidal model.	25
Figure 3.5 Distribution of scalar potential in the homogeneous models; (a) whole body, (b) arm, (c) leg and (d) trunk and head.	27
Figure 3.6 Distribution of the IEF in homogeneous models; (a) whole body, (b) arm, (c) leg and (d) trunk and head.	27
Figure 4.1 Configuration of the human models in vehicle cabin	33
Figure 4.2 Definition of body parts of the model: (a) passenger and (b) driver.....	33
Figure 4.3 Distribution of the magnetic field around the vehicle with different materials: (a) iron, (b) aluminum, and (c) CFRP.	35
Figure 4.4 Distribution of induced electric field in the models of (a) driver and (b) passenger in the vehicle made of (i) iron, (ii) aluminum, and (iii) CFRP.....	37
Figure 5.1 Induced electric field in (right) passenger and (left) driver without post-processing: the vehicle body is comprised of (a) iron and (b) CFRP.....	43
Figure 5.2 Induced electric field of driver's armpit. (a) without post-processing and (b) voxels for skin-to-skin contact is excluded.	43
Figure 5.3 Induced electric field of driver's armpit. (a) without post- processing and (b) voxels for skin-to-skin contact is excluded.	44

Figure 5.4 Induced electric field of driver’s thigh and buttocks. (a) without post-processing
and (b) voxels for skin-to-skin contact is excluded. 44

List of Tables

Table 1.1 Basic restrictions in the ICNIRP 2010 guidelines.	2
Table 1.2 Reference level in the ICNIRP 2010 guidelines.	2
Table 3.1 Comparison of induced electric field obtained using the proposed formula and SPFD & FEM (cuboid model).....	24
Table 3.2 Comparison of induced electric fields in the ellipsoidal model from the proposed formula and the SPFD (Ellipsoidal); (a) definition of γ and (b) γ_n	27
Table 3.3 Comparison of induced electric field from the formula and the SPFD (homogeneous realistic-shaped model); (a) TARO model and (b) Duke model.....	29
Table 3.4 Comparison of induced electric field obtained using the formula and SPFD (inhomogeneous model): (a) Taro model and (b) Duke model	31
Table 4.1 Comparison between calculated magnetic field strength for WPT systems with a transmitting power of 3.7 kW when the body material of the vehicle is composed of (a) Iron, (b) Aluminum, and (c) CFRP	37
Table 4.2 Computed induced electric field value for WPT systems with a transmitting power of 3.7 kW when the body material of the vehicle is composed of (a) Iron, (b) Aluminum, and (c) CFRP.....	39
Table 4.3 Value of coupling factor for different body parts when the body material of the vehicle is composed of (a) Iron, (b) Aluminum, and (c) CFRP	40
Table 5.1 Value of coupling factor for different body parts (a) 99.9%ile and (b) exclusion of skin-to-skin contact and 99.9%ile	48

Chapter 1

Introduction

1.1. Background

Studies on human dosimetry and compliance assessment for low-frequency (LF) electromagnetic fields recently have attracted attention because of the emergence of wireless technology, including wireless power transfer for zero emission vehicles. In LF field exposure (below 100 kHz), electrostimulation caused by an induced electric field in the human body is a dominant factor. In actual scenarios of human exposure to LF near fields, a limb of the human body is mainly exposed (local exposure). The field distribution is then nonuniform. Therefore, the assessment of local and nonuniform exposures is essential.

1.1.1. International Guidelines and Standards for Human to Electromagnetic Field Exposure

Two international guidelines and standards have been mentioned in the documents of the World Health Organization: published by the International Commission on Non-Ionizing Radiation Protection (ICNIRP)[1] [2] and Institute of Electrical and Electronics Engineers (IEEE) International Committee on Electromagnetic Safety Technical Committee 95 [3], [4]. They were designed to protect humans from electrostimulation caused by the induced electric

field up to 5–10 MHz. Table 1.1 shows the internal physical quantities and basic restrictions in ICNIRP 2010. However, assessing the internal physical quantities in humans at lower frequencies (LFs) in a straightforward manner is difficult. Therefore, permissible external field strength, named the reference level, is derived as shown in Table 1.2 for practical assessments. The permissible external field strength is derived assuming that the human standing in free space is exposed to uniform field over the body. Thus, the induced electric field for exposure at the reference level is much lower than the basic restriction.

In the ICNIRP radiofrequency (RF) guidelines [1] and the IEEE C95.1-2019 standard [4], the reference level for local exposure was newly introduced. Thus, considering the consistency between LF and RF guidelines, setting a permissible field strength for nonuniform and local exposures would be preferable, even in the LF range. However, the relaxation of the reference level for local exposure in the IEEE C95.6-2002 standard [5] was based on uniform exposure in a homogeneous ellipsoidal model whose major and minor were determined by representing body parts. In contrast, anatomical models were considered in the ICNIRP LF guidelines [2], whereas no limit for local exposure has been prescribed. However, the ICNIRP LF guidelines will be revised in the near future.

Table 1.1 Basic restrictions in the ICNIRP 2010 guidelines.

	Frequency	Basic restriction (V/m)
All tissue of heads and body	1 Hz – 3 kHz	0.4
	3 kHz – 10 MHz	$1.35 \times 10^{-4} f$

f : Frequency in Hz

Table 1.2 Reference level in the ICNIRP 2010 guidelines.

Frequency	Reference level (A/m)
1–8 Hz	$3.2 \times 10^4 / f^2$
8–25 Hz	$4 \times 10^3 / f$
25–400 Hz	1.6×10^2
400 Hz–3 kHz	$6.4 \times 10^4 / f$
3 kHz–10 MHz	21

f : Frequency in Hz

1.1.2. Compliance Assessment Standard

The International Electrotechnical Commission (IEC) is an international standard body that publishes compliance assessment standards for electrical and electric technologies. The IEC is composed of some technical committees (TC) for technology specialties—TC47 (semiconductor devices) and TC69 (electric road vehicles and electric industrial trucks)—to discuss compliance assessment standards. TC106 has discussed some compliance assessment standards for human exposure to LF fields. Regarding human exposure, manufacturers refer to the compliance assessment standards for the assessment methods and the ICNIRP or IEEE for the limit of the reference level and the basic restriction to guarantee product safety. A typical compliance assessment procedure for LF field exposure has three steps (Fig. 1.1) for local and nonuniform exposures.

In the first step, manufacturers measure the external magnetic field at the area defined in the compliance assessment standards (i.e., IEC Technical Specification (TS) 62764-1 defines 20 cm as the measurement distance from the surface of the equipment under study) using a loop coil. Then, the external magnetic field strength is compared with the reference level defined in the ICNIRP or IEEE. If the external magnetic field strength exceeds the reference level, the second step should be performed.

In the second step, the value of the external magnetic field, which is multiplied by a coupling factor, is compared with the reference level. A coupling factor is a scheme developed to analyze human exposure to nonuniform fields at LFs. The formula of the coupling factor is shown in Section 2.4.3. If the strength of the external magnetic field, which is multiplied by a coupling factor, exceeds the reference level, the third step should be performed.

In the third step, the induced electric field is compared with the basic restriction. As described in Section 1.1.1, manufacturers should calculate the induced electric field from the magnetic field distribution, which is measured or calculated using a computational method.

Manufacturers mainly perform the first and second steps. Although the induced electric field in the human body can be calculated at research institutions, compliance assessments for manufacturers should be easier and more practical in the third step. Therefore, the assessment

procedure using a coupling factor for nonuniform exposure was defined in the IEC 62233 (measurement methods for electromagnetic fields of household appliances and similar apparatus regarding human exposure) in the second step [6], [7]. Recently, some IEC standards, i.e., IEC Publicly Available Specification 63184 [8], refer to compliance with a coupling factor. Assessments using a coupling factor can be easily performed since they are performed only by multiplying the external magnetic field by the coupling factor. However, the method for calculating the coupling factor is not considered in the ICNIRP guidelines and IEEE standards, and then, the method for predicting the induced electric field from the external magnetic field distribution for local and nonuniform exposures is needed in a straightforward manner.

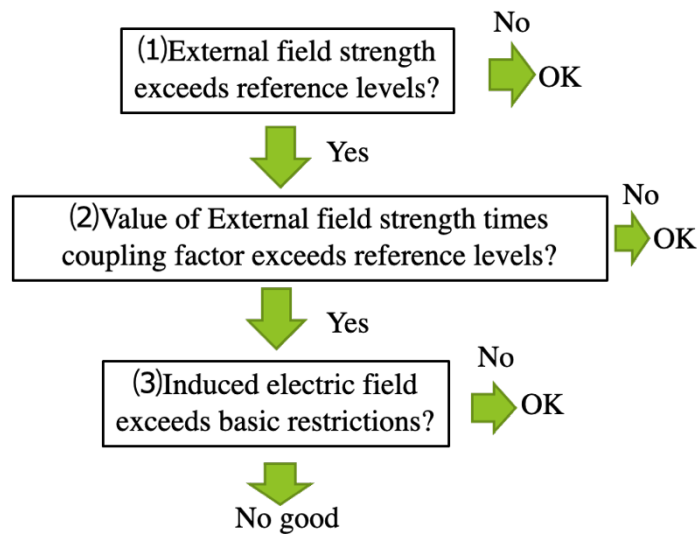


Figure 1.1 Assessment procedure for low-frequency exposure

1.1.3. Review of Previous Studies and Research

Necessity

Concerns on human protection in vehicles

The number of zero-emission vehicles (ZEVs), that is, battery electric vehicles and fuel cell electric vehicles, has increased worldwide. The leaked electromagnetic field in these types of vehicles is larger than that in conventional gasoline/diesel vehicles because of electronization. The frequency of emission from ZEVs ranges from almost direct current to several kHz [9], [10]. Moreover, wireless power transfer (WPT) systems are attractive in the automotive industry, and the frequency of transfer power is 78 kHz. Restrictions against stimulation should therefore be considered. The IEC TC106 decided to establish Project Team (PT) 62764-1 to determine the measurement procedure for the magnetic field levels generated by electronic and electrical equipment in the automotive environment [11] and PT 63184 to determine the methods for assessing human exposure to electric and magnetic fields from WPT systems [8]. Therefore, there have been increasing concerns throughout the vehicle industry about human protection according to IEC trends.

Over-conservativeness in practical scenarios for LF compliance

The external magnetic field strength is measured and compared with the reference level [1] - [4]. However, the external magnetic field generated from sources in practical scenarios is nonuniform, and several studies have shown that the assessment of the spatial peak field strength may be over-conservative [12], [13]. This conservativeness may be because the reference is derived assuming human exposure to a uniform field in free space. The compliance assessment of the basic restriction is thus needed. In the assessment, assessing the induced electric field at LFs is not straightforward. Therefore, IEC 62233 introduced the coupling factor [6] for practical assessment. Regarding the ICNIRP RF guidelines [1] and the IEEE C95.1-2019 standards [4], the reference level for local exposure was newly introduced. However, the relaxation of the reference level for local exposure in the IEEE C95.6-2002 standards [5] was based on uniform

exposure in a homogeneous ellipsoidal model whose major and minor were determined by representing body parts. In contrast, anatomical models were considered in the ICNIRP LF guidelines [2], whereas no limit for local exposure has been prescribed. Therefore, the variation in the induced electric field due to differences in the shape of human body models and model inhomogeneity should be evaluated.

Relationship between external magnetic field and induced electric field

The coupling factor varies depending on the magnetic field distribution and human posture, which is exposed [14], [15], [16]. However, the IEC standards defined one value of the coupling factor for local and nonuniform exposures [8]. Therefore, the method for calculating the coupling factor from the external magnetic field distribution or for predicting the induced electric field from the external magnetic field distribution is needed for local and nonuniform exposures. The relationship between the induced electric field and the basic restrictions for exposure at the reference level has also been discussed in several studies [16] - [24]. However, no study has attempted to calculate the induced electric field from the external magnetic field. This study helps assess local and nonuniform exposure compliance in the ICNIRP, IEEE, and IEC.

Effect of post-processing of the induced electric field

The effects of post-processing of the induced electric field should be evaluated. In computational dosimetry to calculate the induced electric field in the third step in Figure 1.1, the stair-casing approximation of human models, which may include segmentation error, may result in a significant error if pre-/post-processing is not appropriately performed [25]. Therefore, a statistical approach, that is, 99th percentile value of uniform exposure in the ICNIRP or 99.9th percentile of our previous proposal [26], is needed for nonuniform exposure, which is to suppress computational artifacts that are inherent when using voxelized anatomical models. Furthermore, skin-to-skin contact, which is caused by the finite resolution of human models, also produces a locally high electric field [27], whereas it is unessential to cause the stimulation. This is attributed partly to the stair-casing approximation or finite discretization resolution and to the

low conductivity of the skin. In 2019, the revised IEEE C95.1 standards recommend excluding part of skin-to-skin contact [4]. Clarifying the difference in the combination of the post-processing (99.9th percentile and skin-to-skin contact exclusion) for nonuniform and local exposures in realistic postures is necessity.

1.2. Contents of Thesis

This study evaluated the external magnetic field, the electric field induced in the human body and the coupling factor defined in IEC 62233 using an electromagnetic solver from the viewpoint of LF compliance assessment. The motivations of this study were as follows:

1. To propose a method for predicting the induced electric field from the relationship between the uniform external magnetic field and the induced electric field in different body part models to help set the permissible field strength for local exposure.
2. To investigate the relationship between the external magnetic field, the induced electric field, and the coupling factor in the human body for WPT systems, which are implemented on a vehicle body, and discuss the current compliance assessment for local and nonuniform exposures in practical exposure scenarios.
3. To evaluate the effects of post-processing for calculating the induced electric field to clarify the differences between the combination of the post-processing (99.9th percentile and skin-to-skin contact exclusion) for local and non-uniform exposure scenarios in realistic postures.

The contents of this thesis were as follows

Chapter 1 introduces the background and motivation of this study.

Chapter 2 explains the numerical human models, WPT system, and computational methods. First, the cuboid, ellipsoidal, and anatomical human models and WPT systems, which are implemented on the vehicle, are presented. Next, the scalar potential finite difference method

and COMSOL for calculating the induced electric field in numerical models and the coupling factor, respectively, are explained.

Chapter 3 proposes a formula for estimating the induced electric field from the uniform external magnetic field for local exposure. First, a uniform LF magnetic exposure is considered for different body parts to propose a formula in which an induced electric field can be derived in a scenario where the cuboid body part model is exposed to a uniform LF magnetic field. Then, the effectiveness of the formula for homogeneous ellipsoidal models is examined. Finally, the variation in the induced electric field due to differences in the shape of the human body model and model inhomogeneity is calculated.

Chapter 4 computes the external magnetic field, the induced electric fields, and the coupling factor to assess compliance for a WPT system. The vehicle body is composed of iron, aluminum, and carbon fiber-reinforced plastic. This chapter clarifies over-conservativeness for local and nonuniform exposures in practical exposure scenarios and confirms the necessity of this study.

Chapter 5 computes the induced electric field and the coupling factor when the exclusion of skin-to-skin contact defined in IEEE C95.1-2019 is added to the 99.9th percentile value post-processing to clarify the effects of skin-to-skin contact on the induced electric field and the coupling factor.

Chapter 6 shows the summary of this study.

Chapter 2

Models and Methods

2.1. Overview

In this study, we compute the magnetic field, the induced electric field, and the coupling factor for LF exposure. In general, at frequencies lower than the MHz range, a magneto-quasi-static approximation is applicable for the computation of the induced electric field in biological tissues [28]. Under this assumption, the external electric and magnetic fields can be decoupled, and the magnetic field is assumed to be unperturbed by the existence of the human body. Therefore, a two-staged computational approach can then be applied.

In the first stage, the magnetic field is computed by a commercial electromagnetic simulator without considering the human body model for actual scenario. In this study, HFSS (High Frequency Electromagnetic Field Simulation, ANSYS) is used at Chapter. 4 and 5 because of the complex magnetic field distribution generated from WPT system. The distribution of the magnetic vector potential is obtained, and then used as a wave source in the second stage.

In the second stage, the induced electric field is computed by substituting the vector potential distribution into an electromagnetic solver. The solver we use for computing the induced electric field is based on the Scalar-potential finite difference (SPFD) method. At chapter 3, we also use the commercial COMSOL software (COMSOL AB, Stockholm) for computing the induced electric field.

This chapter describes the numerical human models, the WPT system, and computational methods.

2.2. Numerical Human Body Model

2.2.1. Cuboid and Ellipsoidal Model

We use cuboid and ellipsoidal models at Chapter 3 in this study. Figure 2.1 shows a two-layer cuboid model. The cuboid model consists of skin and muscle because the skin of human body model was chosen as worst case target tissue in ICNIRP guideline. The size of the cuboid model was $(\alpha, \beta, \gamma) = (0.4 \text{ m}, 0.4 \text{ m}, 0.1\text{--}2.0 \text{ m})$ in Figure 2.1.

Homogeneous ellipsoidal model (two dimensional) are defined in IEEE C95.6-2002 [5], wherein the major and minor axes are determined for the corresponding body parts. Three sizes of the homogeneous ellipsoidal model were considered Figure 2.1 (c). The sizes of the major and minor axes were $(a, b) = (0.90 \text{ m}, 0.17 \text{ m})$ for the whole body, $(0.40 \text{ m}, 0.17 \text{ m})$ for the trunk and head, and $(0.42 \text{ m}, 0.09 \text{ m})$ for the leg.

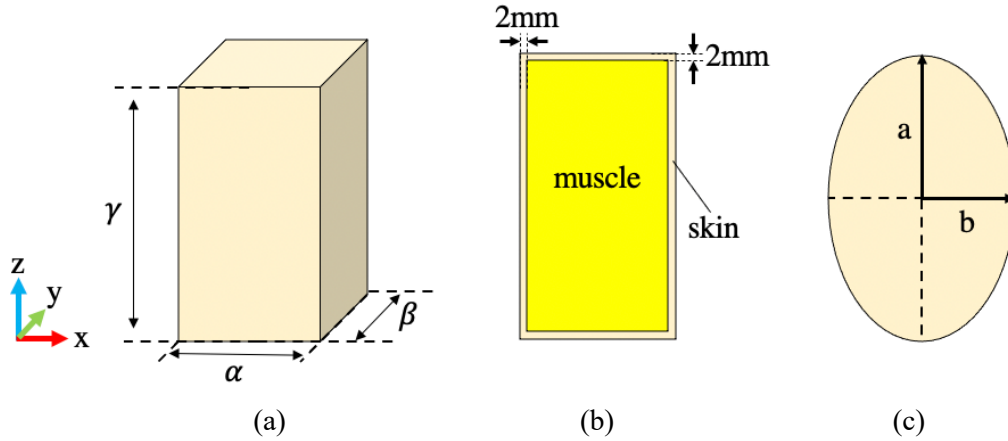


Figure 2.1 Schematic explanation of model: (a) cuboid model, (b) tissue composition of cuboid model and (c) ellipsoidal model

© 2021 IEEE

2.2.2. Anatomical Model

TARO and Duke models which were developed at the National Institute of Information and Communications Technology (NICT) and IT'IS Foundation, respectively, are used as numerical anatomical human body. Duke model is used at Chapter 3 to compare the induced electric fields of TARO model. The inhomogeneous and homogeneous anatomical models are also used.

The original inhomogeneous TARO and Duke model consist of 51 and 77 tissues, respectively. The electrical conductivity of the homogeneous anatomical model is set to $2/3$ of muscle based on an approximate ratio of high and low water content tissue of 2 : 1 [29], which is also used at Chapter 3.

The whole body of the original inhomogeneous TARO model is also divided into the trunk and head, arm, and leg in Chapter 4 and 5 as shown in Figure 2.3 to assess the compliance assessment method (IEC TS 62764-1) [11].

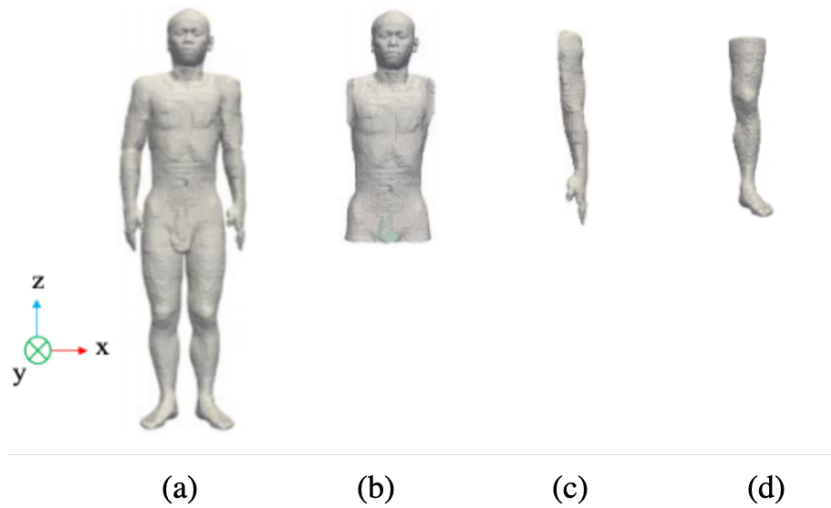


Figure 2.2 Schematics of anatomical human body model: (a) whole body, (b) head and trunk, (c) arm and (d) leg.

© 2021 IEEE

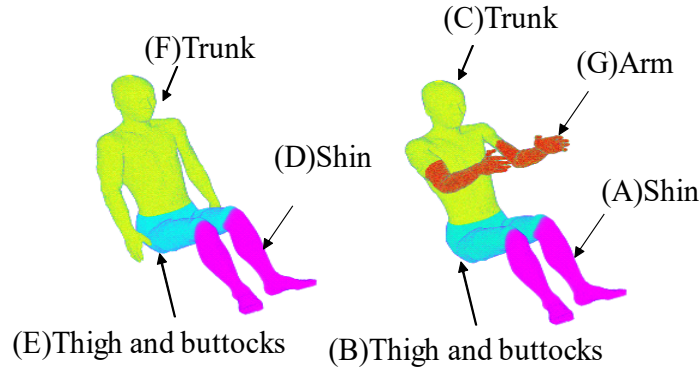


Figure 2.3 Definition of body parts of the model: (a) passenger and (b) driver.

© 2019 IEEE

2.3. WPT System

2.3.1. Schematic Diagram of WPT System

A vehicle model for which the WPT system is implemented is shown in Figure 2.4, which is used at Chapter 4. As shown in Figure 2.4, the geometry of the simplified vehicle is developed based on Prius of Toyota Motor Corporation. The vehicle is placed in free space. A receiving coil is installed below the center of the vehicle body. The transmitting coil is modeled assuming that it is installed in the parking area. The misalignment of the receiving and transmitting coils were chosen as 75 mm and 100 mm in the x and y directions, respectively, based on Society of Automotive Engineers (SAE) J2954 [30]. The reason for the misalignment is that the leaked magnetic field strength has a larger value than that in the face-to-face position, which is attributable to the increment of the coil current [31].

We compare the effects of three materials for the vehicle body: iron, aluminum, and carbon fiber reinforced plastic (CFRP). The relative permittivity, permeability, and conductivity of iron,

aluminum, and CFRP are $(1, 4000, 10.3 \times 10^6 \text{ S/m})$, $(1.000021, 1.000021, 38 \times 10^6 \text{ S/m})$, and $(1, 1, 0.25 \times 10^6 \text{ S/m})$, respectively. The thickness of iron, aluminum and CFRP is 0.5 mm, 1.0 mm, and 2.0 mm, respectively. The iron permeability of 4000 is assumed as constant because the magnetic field strength at vehicle body is less than 1000A/m where the iron is considered as linear material [32]. Finite conductivity boundary for vehicle body, perfect conductor boundary for ground floor and coils, perfect matched layer in free space is used.

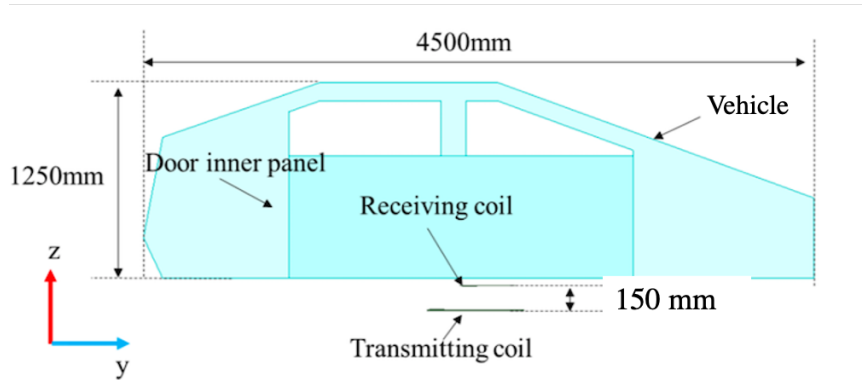


Figure 2.4 Schematic diagram of WPT vehicle

© 2020 IEEE

2.3.2. WPT Coil

A detailed schematic diagram for the WPT coils is shown in Figure 2.5. The shape and dimension of each coil is modeled based on [30]. The transmitting coil has a rectangular shape with a length of 640 mm and a width of 500 mm. The number of turns of the transmitting coil is 15 and the width is 3 mm. The receiving coil is a 320 mm square. The receiving coil has 20 turns and a width of 2 mm. The transmitting distance is 150 mm between the top of transmitting coil and the bottom of the receiving coil. These parameters are based on the definition in the documents of SAE J2954 [30]. Each coil is composed of a perfect conductor. The transmitting coil and the receiving coil have just current sources of 16 A and 17 A, respectively, to transfer a transmitting power of 3.7 kW. The current phase difference is 90 deg. The frequency of the WPT system is 85 kHz. The current sources are calculated with equation (8) in [33].

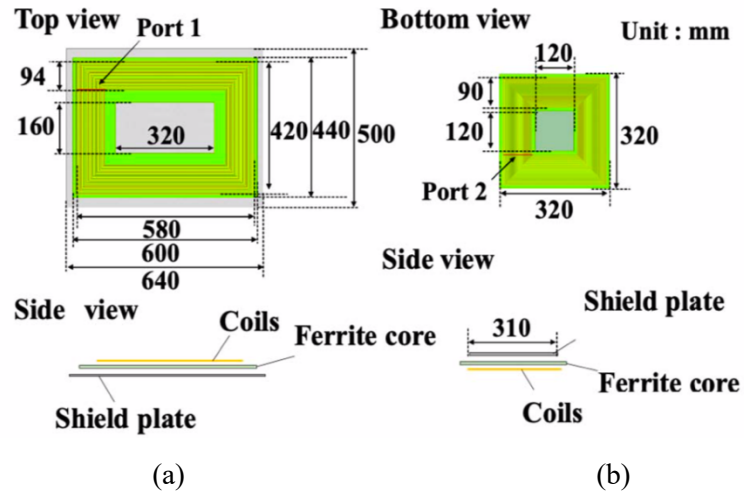


Figure 2.5 Schematic diagram of WPT coils: (a) transmitting and (b) receiving coils

© 2020 IEEE

2.4. Computational Methods

2.4.1. Induced Electric Field

SPFD

In this study, we use SPFD method [34] to calculate the induced electric field. The SPFD which was developed at Nagoya Institute of Technology is widely adopted LF magnetic exposure dosimetry [34], [35]. The induced electric field can be calculated by follows:

$$\mathbf{E} = -\nabla\phi - j\omega\mathbf{A} \quad (2.1)$$

where ϕ is the unknown scalar potential and \mathbf{A} is the vector potential which is satisfied with follows:

$$\mathbf{B} = \nabla \times \mathbf{A} \quad (2.2)$$

We use the magnetic flux density \mathbf{B} which is calculated by the commercial electromagnetic simulator (HFSS) which uses the finite element method (FEM) using tetrahedral meshes, because of the practical exposure scenarios at Chapter 4 and 5. At Chapter 3, we defined the vector potential because of simple uniform exposure scenario (See 3.3.1).

We then calculate the scalar potential by solving simultaneous linear equations using the SPFD method as follows:

$$\sum_{n=1}^6 s_n \varphi_n - \left(\sum_{n=1}^6 s_n \right) \varphi_0 = j\omega \sum_{n=1}^6 (-1)^n s_n l_n A_{0n} \quad (2.3)$$

where s_n is edge conductance, φ_n is Scalar potential at each node, l_n is edge length of the voxel, and n is node position label. The geometric multigrid method was used to accelerate the convergence [35]. The size of the cubical voxels was 2 mm in this study.

COMSOL

In this study, we also use COMSOL at Chapter 3 to compare the induced electric field of Cuboid and ellipsoidal models, which is calculated by SPFD method. The COSMOL software uses the FEM in calculating the induced electric field using tetrahedral meshes [36]. Notably, although the models based on tetrahedral meshes are insensitive to stair-casing errors, the quality of the meshes affects the computations of the maximum induced electric fields. In this study, the body model was automatically meshed, determined by workstation memory. The mesh sizes of the cuboid and homogeneous ellipsoidal models were less than 1.8 (nonuniform mesh distribution) and 1.2 cm, respectively, which was determined by the limited workstation memory.

2.4.2. Post-processing Algorithm

In computational dosimetry, the stair-casing approximation of human models, which may include segmentation error, may result in a significant error if pre-/post-processing is not appropriately performed [25]. In addition, the skin-to-skin contact also produces a locally high electric field [27], whereas it is not essential to cause the stimulation. This is attributed partly to the stair-casing approximation or finite discretization resolution, and partly to the low conductivity of the skin. A previous computational study also suggested that the electrostimulation threshold was not almost changed for scenarios in which the enhancement of the induced electric field due to the skin-to-skin contact is expected in computation, and that the weakness of the skin modeling is the primary reason [37]. Therefore, skin-to-skin contact was excluded in this study according to the revised IEEE C95.1 standard in 2019, which recommended that the parts of skin-to-skin contact, or corresponding the induced electric field, should be excluded. The effect of the exclusion of skin-to-skin contacts shows in Chapter 5.

We firstly exclude the locally high induced electric field at skin-to-skin contact from the induced electric field distribution on the surface of the human body model, and then employ the 99%ile which is defined in ICNIRP 2010 [2] or 99.9%ile values which is proposed previous

study [26]. Chapter 3 employs the peak voxel value for the cuboid and homogeneous ellipsoidal models and the 99%ile and 99.9%ile values for each body part in the anatomical human body. Chapter 4 and 5 employs 99.9%ile values for each body part in the anatomical human body because the previous proposal for nonuniform exposure [26] is adopted.

2.4.3. Coupling Factor

We use the coupling factor for analyzing human exposure to nonuniform fields at Chapter 4 and 5. The general idea behind the coupling factor is defined in IEC 62233. The spatial-peak magnetic field strength which is measured or calculated is multiplied by the coupling factor which value is defined in the compliance assessment standards, is compared with the reference level in the second step of the compliance assessment. The coupling factor can be calculated by follows:

$$a_c = \left(\frac{E_{max}}{H_{max}}\right) / \left(\frac{E_{BR}}{H_{RL}}\right) \quad (2.4)$$

Where E_{max} is the peak value of the induced electric field which is calculated from the SPFD. E_{BR} and H_{RL} is the basic restriction and the reference level prescribed in the ICNIRP or IEEE. In this study, the basic restrictions and the reference level of ICNIRP 2010 is used, respectively, as shown in Table 1.1 and Table.1.2. H_{max} is the spatial maximum value of the magnetic field strength. In this study, the magnetic field is computed in the computational domain averaged over 100 cm². The area of 100 cm² assumes the 100 cm² loop antenna which is used to measure the magnetic field in the first step of the compliance assessment (See Figure 1.1).

Chapter 3

A Method for Predicting the Induced Electric Field for Local Exposure

3.1. Overview

In this chapter, we discuss the relationship between uniform external magnetic field strength and induced electric field in different body part models to help set the permissible field strength for the local exposure. We proposed a formula for predicting the induced electric field from electromotive force from cuboid models based on Faraday's law. Then, we applied the formula to homogeneous ellipsoidal and homogeneous realistically shaped models to examine the effectiveness of the proposed formula. Further, we investigated the effect of model inhomogeneity to confirm the difference in the induced electric field in anatomical body models. The computational results show that the homogeneous ellipsoidal model was comparable to the homogeneous realistically shaped model, whereas the model inhomogeneity led to approximately 1.5 times increase in the computed maximum electric field strength. The results presented here were published in [38].

© 2021 IEEE. Reprinted, with permission, from K. Miwa, "A Novel Method to Predict the Maximum Electric Fields in Different Body Parts Exposed to Uniform Low-Frequency Magnetic Field", IEEE Transactions on Electromagnetic Compatibility, Aug. 2021.

3.2. Exposure Scenario

The magnetic field was a spatially uniform field of 0.1 mT at 100 Hz, and was in the anterior posterior direction (y direction in Figure 2.1 and Figure 2.2) for all scenarios considered in this chapter. Thus, the cross-sectional area perpendicular to the magnetic field was the largest, resulting in the highest induced electric field strength, based on Faraday's law as well as from [39]. For anatomical models, highest induced electric field were also consistently found for this exposure scenario [40]. This scenario is the same as considered in the international guidelines and standard.

3.3. Results

3.3.1. Derivation of Empirical Formula

In this section, cuboids were used to determine the relationship between the external magnetic field and the induced electric field in different body parts to develop an empirical formula by which the induced electric field can be simply estimated from the external magnetic field.

Maximum Induced Voltage

For LF exposure, using Faraday's law, the total induced voltage, i.e., the electromotive force is expressed as follows:

$$V_{in} = \omega \iint \mathbf{B} \cdot \mathbf{n} dS = \omega BS \quad (3.1)$$

where $\omega = (2\pi f)$ is the angular frequency of the magnetic field, \mathbf{B} is the magnetic flux density, S is the projection area wherein the magnetic field flows into a human body, and \mathbf{n} is the unit

vector on S . Then, the maximum induced voltage in the body model is determined by the projected area of the human body in the same direction because ω and B are constant.

Distributions of Scalar Potential and Electric Field

The induced electric field can be determined by eq. (2.1) in chapter 2. In this scenario in Chapter 3, vector potential \mathbf{A} of eq. (2.2) was defined as follows:

$$\begin{aligned} A_x &= B \cdot z \\ A_y &= 0 \\ A_z &= 0 \end{aligned} \tag{3.2}$$

The computed distributions of the scalar potential ϕ inside the cuboid model are shown in Figure 3.1 (a). The induced electric field shown in Figure 3.1 (b) are obtained by the following:

$$\begin{aligned} E_x &= -\frac{d\phi}{dx} - j\omega A_x \\ E_y &= -\frac{d\phi}{dy} \\ E_z &= -\frac{d\phi}{dz} \end{aligned} \tag{3.3}$$

As seen from Figure 3.1 (b), the maximum induced electric field is dominated by z component and appeared at the center of the two long edges of the model. In addition, the maximum induced electric field, E_z , is only related to scalar potential ϕ . The induced electric field distribution shows the same tendency as experimental results [41].

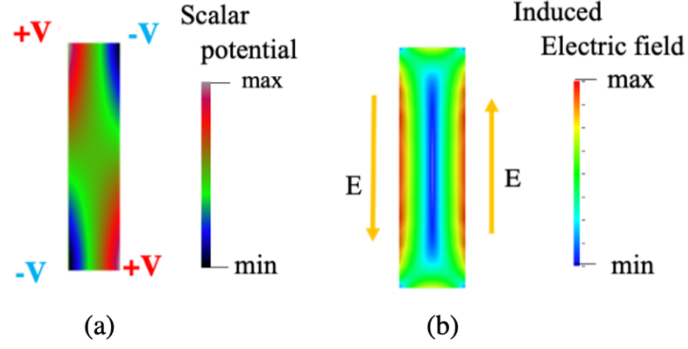


Figure 3.1 Distribution of (a) scalar potential and (b) electric field electric field computed using the SPFD method; $\alpha = 0.4$ m, $\gamma = 1.2$ m.

© 2021 IEEE

Then, we examined the relationship between V_{in} and maximum induced electric field using the cuboid model with varying side lengths, γ . The normalized scalar potential (normalized to V_{in}) along the long side of the cuboid model is shown in Figure 3.2; the scalar potential was close to a linear function of z , especially for models with large aspect ratios. The maximum electric field was equal to the slope of the orange dashed line in Figure 3.2, i.e., $E_{max} = \Delta V / \gamma$, where ΔV is the difference in scalar potential between the two ends of the edge (Figure 3.2 (b)). In addition, ΔV was slightly lower than $V_{in} / 2$ and approached $V_{in} / 2$ with the increase in the slide length of the cuboid model, γ .

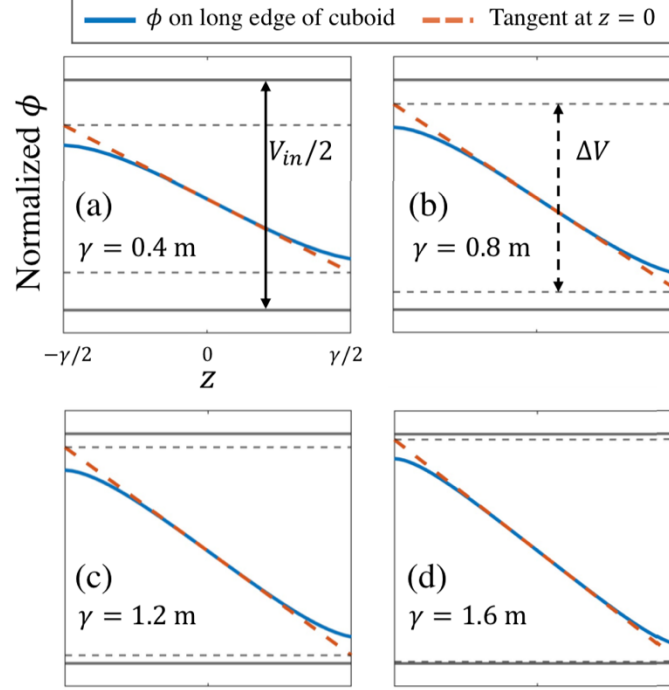


Figure 3.2 Normalized scalar potentials on the long edge of the cuboid model for (a) $\gamma = 0.4$ m, (b) $\gamma = 0.8$ m, (c) $\gamma = 1.2$ m, and (d) $\gamma = 1.6$ m. $\alpha = 0.4$ m.

© 2021 IEEE

Formula of Induced Electric Field

The above analysis suggested that the maximum electric field, which appeared at the longer edge of the cuboid, can be estimated with a simple formula in terms of V_{in} . This approach consists of two steps.

Step 1: Obtain the maximum induced voltage based on Faraday's law.

Step 2: The maximum voltage at the long side of the cuboid model was calculated as half of V_{in} , the maximum electric field was estimated to be the ratio of $0.5V_{in}$ to the length of the long edge of the cuboid.

In step 2, the maximum induced electric field are obtained by follows;

a) $\gamma < \alpha$

$$E_{max} = V_{in} / 2 = \omega BS / 2\alpha \quad (3.4)$$

b) $\gamma \geq \alpha$

$$E_{max} = V_{in} / 2 = \omega BS / 2\gamma \quad (3.5)$$

3.3.2. Comparison Between Formula and SPFD & FEM for Cuboid Model

The calculated induced electric field strengths in the cuboid are listed in Table 3.1 for different values of γ . In Table 3.1, E_{max}^{est} represents the estimated maximum electric field by the proposed formula, E^{num} represents the electric field numerically obtained by SPFD or FEM. The “num/est” represents the ratio of the maximum electric obtained by SPFD or FEM to that estimated by the proposed formula.

From Table 3.1 when the aspect ratio of the cubic is not less than 2:1, the difference in the maximum electric fields obtained from the proposed formula and SPFD was less than 8%, and that from the FEM results was less than 7%. When the two side lengths were comparable, the difference increased to approximately 33%.

Table 3.1 Comparison of induced electric field obtained using the proposed formula and SPFD & FEM (cuboid model)

α	β	γ	E_{max}^{est} [mV/m]	SPFD		FEM	
				E^{num} [mV/m]	num/est	E^{num} [mV/m]	num/est
0.4	0.4	0.1	3.14	3.07	0.98	3.19	1.01
		0.2	6.28	5.79	0.92	5.85	0.93
		0.4	12.6	8.42	0.67	8.51	0.68
		0.8	12.6	11.6	0.92	11.7	0.93
		1.6	12.6	12.5	0.99	12.5	0.99
		2.0	12.6	12.5	0.99	12.6	1.00

© 2021 IEEE

To determine the cause of this difference, the distributions of the induced electric field and scalar potential for these parameters are analyzed (Figure 3.3). As shown in Figure 3.3 (a), the induced electric field had a maximum value at the center of each side of the cuboid. The scalar potential distributions were similar to those for the rectangle model in Figure 3.1 (a), as the electromotive force was evenly distributed on the four edges of the rectangular model. Therefore, the induced electric field obtained from SPFD or FEM for $\gamma = 0.4$ m was lower than that of the proposed formula, which would be a limitation of the formula under specific conditions. These results verified the proposed formula and the computation using the SPFD and FEM.

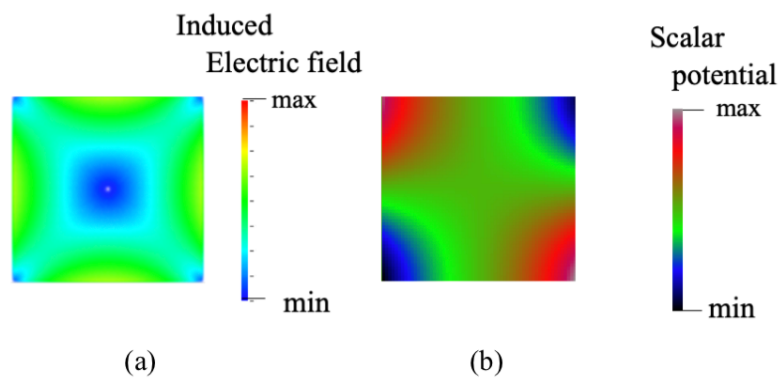


Figure 3.3 Distribution for cuboid with $\alpha = \gamma = 0.4$ m (SPFD); (a) IEF and (b) scalar potential.

© 2021 IEEE

3.3.3. Effect of Model Shape

The induced electric fields calculated from the proposed formula, SPFD, and FEM were compared in the homogeneous ellipsoidal and homogeneous realistically shaped models. The distributions of the scalar potential and the induced electric field in the homogeneous ellipsoidal model are shown in Figure 3.4; the results for the induced electric field in the homogeneous ellipsoidal model are shown in Table 3.2 (a). In Figure 3.4, the distributions of the scalar potential and the induced electric field are similar to those of the cuboids (see Figure 3.1). In Table 3.2 (a), the S is the projection area that the magnetic field flows through the model. α and γ in eq. (3.4) and (3.5) were simply defined as the side lengths of the minimum bounding rectangle of the homogeneous ellipsoidal model (Figure 3.4 (a)). Because $\alpha < \gamma$, the induced electric field could be obtained by eq. (3.5). As shown in Table 3.2 (a), the difference in the induced electric field between the SPFD and proposed formula was less than 40% and 31% for 100%ile and 99.9%ile, respectively. Similar tendencies were found compared with FEM results. Therefore, to improve the results of the proposed formula, we defined γ_n as the intersections of the ellipsoidal circumference and two diagonals of the bounding rectangle (see the yellow solid and dashed lines in Figure 3.4 (a)), which coincide with the maximum and minimum scalar potentials (indicated by orange circles in Figure 3.4 (a)). As shown in Table 3.2 (b), the difference in the induced electric field between the SPFD and proposed formula was less than 9% and 15% for 100%ile and 99.9%ile, respectively. The induced electric field from the FEM was less than that of the SPFD for both 100%ile and 99.9%ile values because the FEM solution did not result in the staircasing error.

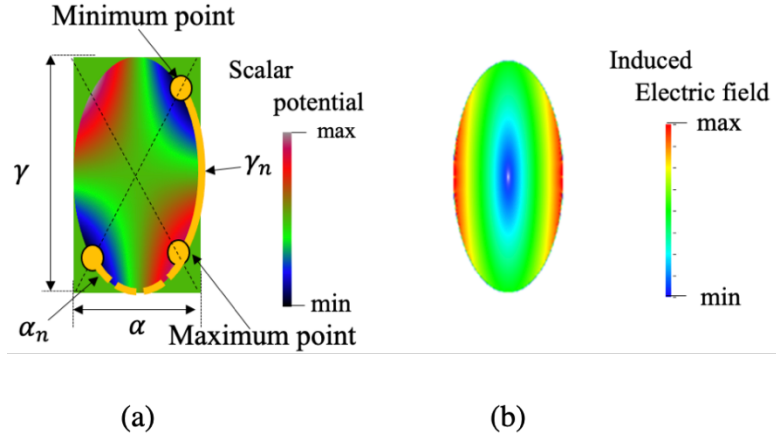


Figure 3.4 Distribution of (a) scalar potential and (b) IEF in ellipsoidal model.

© 2021 IEEE

Table 3.2 Comparison of induced electric fields in the ellipsoidal model from the proposed formula and the SPFD (Ellipsoidal); (a) definition of γ and (b) γ_n

(a)

Model	γ [m]	S [m ²]	E_{max}^{est} [mV/m]	SPFD				FEM			
				E^{num} [mV/m]		num/est		E^{num} [mV/m]		num/est	
				100 %ile	99.9 %ile	100 %ile	99.9 %ile	100 %ile	99.9 %ile	100 %ile	99.9 %ile
Whole body	1.80	0.481	8.36	11.7	10.6	1.40	1.26	10.3	10.1	1.23	1.20
Trunk and head	0.90	0.214	8.26	10.2	9.56	1.23	1.15	9.05	8.90	1.10	1.08
Left leg	0.84	0.119	4.31	5.95	5.66	1.36	1.31	5.41	5.20	1.26	1.21

(b)

Model	γ_n [m]	S [m ²]	E_{max}^{est} [mV/m]	SPFD				FEM			
				E^{num} [mV/m]		num/est		E^{num} [mV/m]		num/est	
				100 %ile	99.9 %ile	100 %ile	99.9 %ile	100 %ile	99.9 %ile	100 %ile	99.9 %ile
Whole body	1.32	0.481	11.4	11.7	10.6	1.03	0.93	10.3	10.1	0.90	0.89
Trunk and head	0.59	0.214	11.2	10.2	9.56	0.91	0.85	9.05	8.90	0.81	0.79
Left leg	0.60	0.119	6.03	5.95	5.66	0.99	0.94	5.41	5.20	0.90	0.86

© 2021 IEEE

The distributions of the scalar potential and the induced electric field in the homogeneous TARO model are shown in Figure 3.5 and Figure 3.6, respectively. The results for the induced electric field in the homogeneous TARO and Duke models are listed in Table 3.3, wherein S is

the projection area that the magnetic field through the model. Because of the complex shape of the anatomical models, α and γ in eq. (3.4) and (3.5) were also defined for simplicity and clarity as the side lengths of the minimum bounding rectangle of the anatomical model (Figure 3.5). Because $\alpha < \gamma$, the induced electric field could be obtained by eq. (3.5). In Table 3.3 (a), the induced electric field obtained using the proposed formula for the TARO model showed a similar trend to that of the SPFD. The largest induced electric field was observed for the whole body, followed by the trunk and head, left leg, and left arm. The difference in the results obtained from the proposed formula and SPFD was less than 29% and 12% for 99.9%ile and 99%ile, respectively.

As shown in Table 3.3 (b), the difference in the results obtained from the proposed formula and SPFD for the Duke model was less than 27% and 9% for 99.9%ile and 99%ile, respectively. Therefore, we confirmed that the proposed formula could be used to calculate the 99%ile value of the induced electric field in the homogeneous part model. In addition, as shown in Table 3.2 and Table 3.3, the 99.9%ile values in the homogeneous ellipsoidal model were similar to those in the homogeneous model.

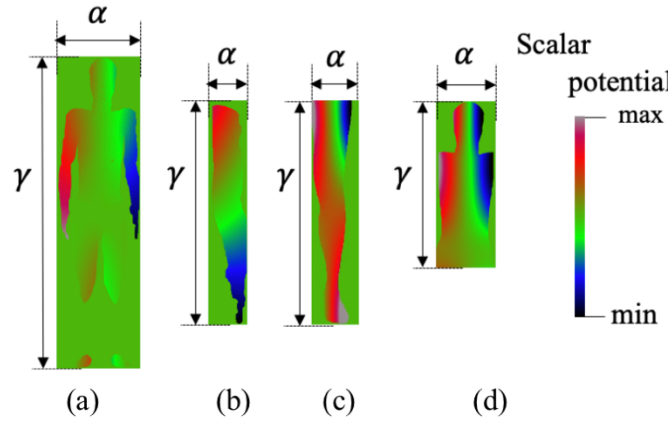


Figure 3.5 Distribution of scalar potential in the homogeneous models; (a) whole body, (b) arm, (c) leg and (d) trunk and head.

© 2021 IEEE

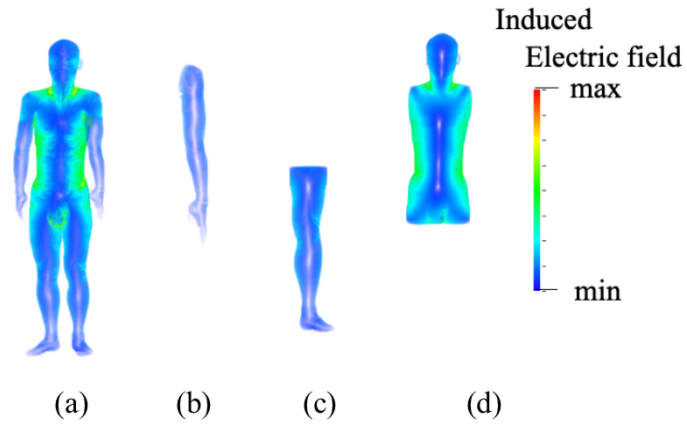


Figure 3.6 Distribution of the IEF in homogeneous models; (a) whole body, (b) arm, (c) leg and (d) trunk and head. © 2021 IEEE

Table 3.3 Comparison of induced electric field from the formula and the SPFD (homogeneous realistic-shaped model); (a) TARO model and (b) Duke model.

(a)

Model	Model Size		E_{max}^{est} [mV/m]	E^{num} [mV/m]		num/est	
	γ [m]	S [m ²]		99.9%ile	99%ile	99.9%ile	99%ile
Whole body	1.732	0.542	9.83	11.5	8.79	1.17	1.09
Trunk and head	0.930	0.248	8.37	9.49	8.13	1.13	0.97
Left leg	0.710	0.086	3.73	4.34	3.84	1.16	1.03
Left arm	0.732	0.053	2.28	2.93	2.54	1.29	1.12

(b)

Model	Model Size		E_{max}^{est} [mV/m]	E^{num} [mV/m]		num/est	
	γ [m]	S [m ²]		99.9%ile	99%ile	99.9%ile	99%ile
Whole body	1.804	0.560	9.76	11.7	9.16	1.20	0.94
Trunk and head	1.020	0.290	8.92	11.2	9.17	1.27	1.03
Left leg	0.784	0.085	3.40	4.03	3.66	1.19	1.08
Left arm	0.768	0.055	2.23	2.77	2.43	1.24	1.09

© 2021 IEEE

3.3.4. Effect of Tissue Inhomogeneity

The induced electric fields calculated from the proposed formula, SPFD, and FEM in the inhomogeneous model were compared to confirm the applicability of the proposed formula. The induced electric field in the inhomogeneous model is presented in Table 3.4.

In Table 3.4 (a), the difference between the results obtained from the proposed formula and SPFD for the TARO model was less than 76% and 23% for 99.9%ile and 99%ile, respectively. In Table 3.4 (b), the difference in the results obtained from the proposed formula and SPFD for the Duke model was less than 103% and 29% for 99.9%ile and 99%ile, respectively. Therefore, the proposed formula could produce a relatively good estimation for the 99%ile value of induced electric field for the inhomogeneous part model.

As shown in Table 3.3 and Table 3.4, the 99.9%ile and 99%ile values for E^{num} in the inhomogeneous model were higher than those in the homogeneous model. The induced electric fields in the inhomogeneous model were approximately 1.5 and 1.2 times higher than that in the homogeneous model for 99.9%ile and 99%ile, respectively.

Table 3.4 Comparison of induced electric field obtained using the formula and SPFD (inhomogeneous model): (a) Taro model and (b) Duke model.

(a)

Model	Model Size		E_{max}^{est} [mV/m]	E^{num} [mV/m]		num/est	
	[m]	S [m ²]		99.9%ile	99%ile	99.9%ile	99%ile
Whole body	1.732	0.542	9.83	17.3	10.6	1.76	1.08
Trunk and head	0.930	0.248	8.37	14.1	10.3	1.69	1.23
Left leg	0.710	0.086	3.73	5.14	4.11	1.38	1.10
Left arm	0.732	0.053	2.28	3.67	2.82	1.61	1.23

(b)

Model	Model Size		E_{max}^{est} [mV/m]	E^{num} [mV/m]		num/est	
	[m]	S [m ²]		99.9%ile	99%ile	99.9%ile	99%ile
Whole body	1.804	0.560	9.76	18.0	11.1	1.84	1.13
Trunk and head	1.020	0.290	8.92	18.1	11.5	2.03	1.29
Left leg	0.784	0.085	3.40	4.80	3.88	1.41	1.14
Left arm	0.768	0.055	2.23	3.20	2.62	1.43	1.17

© 2021 IEEE

3.4. Discussion & Conclusion

This chapter derived a formula to relate the external magnetic field and the induced electric field in human body parts for local exposure. Conservatively, the magnetic field was assumed to be uniform for each body part. Such exposure scenario was adopted by IEEE C95.1 to derive the magnetic field limits from the induced electric field threshold for nonuniform environmental magnetic field. However, such a limit has not been prescribed in the ICNIRP LF guidelines, whereas it was set in the RF guidelines revised in 2020. The motivation for this chapter was to resolve the discrepancy between the two international guidelines and standards and those in the RF. From the computation for the cuboid model, the maximum induced electric field appeared

at the center of the two long edges of the cuboid. The difference in scalar potential between the two ends of the edge was half of the total induced voltage, and the scalar potential on the long edge of the cuboid model was close to a linear function of z . Therefore, the induced electric field could be calculated by dividing half of the total induced voltage with the long side length of the model. Then, we confirmed that the difference between the electric field computed by the proposed formula and SPFD was less than 8%, except for the case where the long and short side lengths were comparable. We evaluated whether the proposed formula could be applied to the homogeneous ellipsoidal model defined in IEEE C95.6-2002. The differences in the induced electric fields—calculated using the proposed formula and SPFD—were less than 9% and 15% for the maximum and 99.9%ile values, respectively.

The induced electric field computed using the FEM showed a similar tendency as that of the SPFD, but the percentile values were approximately 6% less than those of the SPFD, which was due to a smaller mesh number in the FEM than in the SPFD, as the mesh size of the FEM was larger than that of the SPFD due to the limited workstation memory (See 2.4.1). Thus, the volume, excluding the tetrahedral in the FEM, was larger than that of the SPFD. Similarly, the differences in the induced electric field, which was calculated using the proposed formula and FEM, were less than 19% and 21% for the maximum and 99.9%ile values, respectively.

In the realistically shaped homogeneous TARO model, the induced electric fields calculated using the SPFD were larger than those of the analytical estimates by 29% and 12% for 99.9%ile and 99%ile, respectively. In the inhomogeneous model, the induced electric field obtained using the SPFD were 76% and 23% larger than those of 99.9%ile and 99%ile, respectively. Similar results were observed for the Duke model. Therefore, we confirmed that the proposed formula could be used to calculate the 99%ile induced electric field consistently when the size of the human body part is exposed to the external magnetic field, and the external magnetic field strength could be obtained.

In addition, we compared the induced electric fields in the homogeneous ellipsoidal, homogeneous realistically shaped, and inhomogeneous models for the 99.9%ile value. We found that the induced electric field in the homogeneous ellipsoidal model, defined in IEEE C95.6, was similar to that in the homogeneous model, and the induced electric field in the inhomogeneous model was 1.5 times higher than that of the homogeneous model.

Finally, we discuss the coupling factor of eq. (2.4) at left leg of the homogeneous TARO model by using the induced electric field which is obtained from the proposed formula. We found that

the reference level which is defined in ICNIRP 2010 can be relaxed approx. by 50 times because the value of the coupling factor is 0.02 at left leg of the homogeneous TARO model.

These results suggested that the homogeneous ellipsoidal model could be extended for deriving a limit in terms of the induced electric field considering these factors. Thus, a minor revision of the exposure reference level for limbs (partial body) in the IEEE C95.6 standard would provide a more consistent limit. In addition, the ratio will be helpful in deriving the reference level of the ICNIRP guidelines if consistency with the RF guidelines is considered.

Chapter 4

Compliance Assessment for Wireless Power Transfer Systems in Vehicle for Local and Nonuniform Exposure

4.1. Overview

This chapter investigates the relationship between the external magnetic field, the induced electric field, and the coupling factor in human body for WPT systems (3.7 kW) implemented on a vehicle for local and nonuniform exposure. The vehicle body is composed of iron, aluminum, and carbon fiber reinforced plastic (CFRP) to assess the current compliance assessment in practical exposure scenario.

The computational results revealed that when the body of the vehicle is composed of CFRP, the magnetic field strength leaking into the vehicle is higher than that with other materials. The averaged value of the magnetic field strength at the passenger's feet was 1.1 times higher than the reference level of ICNIRP 2010. However, the internal electric field was less than the basic restriction until the magnetic field strength was 11.1 times higher than the reference level. This means that a transmitting power of 370 kW is permitted to comply with the ICNIRP guideline. The coupling factor in the limb (excluding the thigh and buttocks and the trunk) ranged from 0.027 to 0.076. Therefore, nonuniformity of the field is difficult to generalize, and a conservative (larger) coupling factor would be essential.

The results presented here were published in [39].

© 2019 IEEE. Reprinted, with permission, from K. Miwa, “Electromagnetic Dosimetry and Compliance for Wireless Power Transfer Systems in Vehicles”, IEEE Transactions on Electromagnetic Compatibility, Nov. 2019.

4.2. Exposure Scenario

Two positions of realistically postured models were considered: sitting in the driver’s seat and sitting in the passenger’s seat, as shown in Figure 4.1. The distance from the top surface of the receiving coil to the driver’s and the passenger’s buttock was 140 mm. This value assumes a realistic environment of the vehicle, i.e., the feet are on the floor and the thigh and buttocks are on the seat of the vehicle. In this Chapter, we define the body parts as shown in Figure 2.3 which is same definition of IEC TS 62764-1 [11].

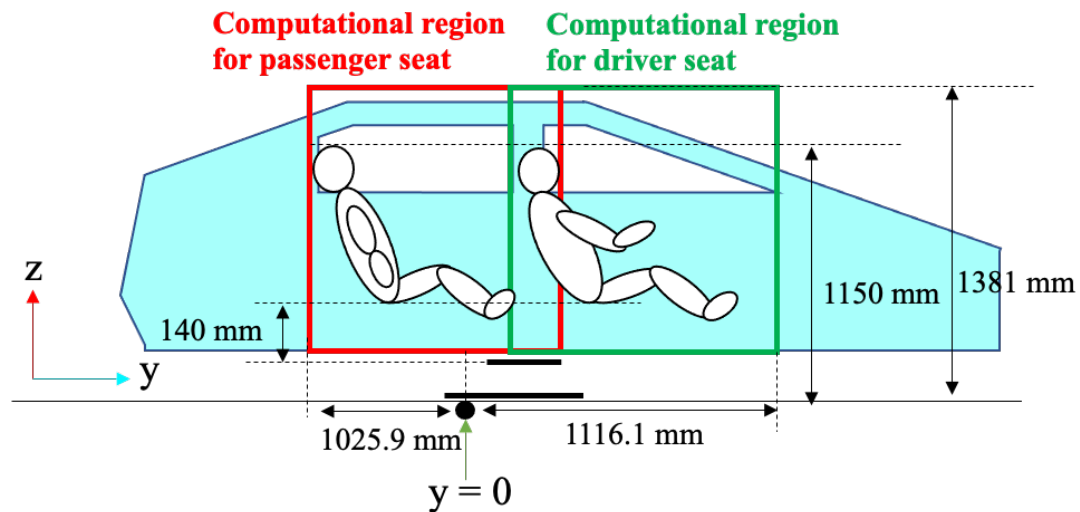


Figure 4.1 Configuration of the human models in vehicle cabin

© 2020 IEEE

4.3. Results

4.3.1. Distribution of Magnetic Field

The distribution of the magnetic field, viewed from the front of the vehicle at $y = 0$ mm (Figure 4.1), is shown in Figure 4.2. The magnetic field leaks from the window into the interior for vehicle bodies made of iron and aluminum. On the other hand, for bodies made of CFRP, the magnetic field generated by the WPT leaks directly into the cabin under the floor. The value of the magnetic field strength is computed in the computational domain of 100 cm^2 . The value of the magnetic field strength is the averaged value of 100 cm^2 and a vector summation of the x , y , and z components. According to Table 4.1, the averaged value of the magnetic field strength at the passenger's feet was 1.1 times higher than the reference level of ICNIRP 2010 in Table 1.2, even for CFRP in which the magnetic field strength at the human model position was the highest among the three materials.

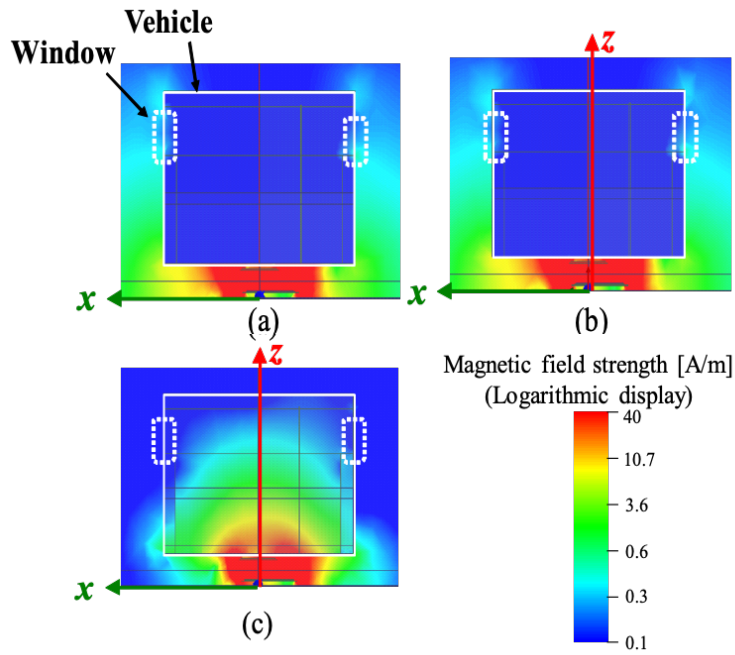


Figure 4.2 Distribution of the magnetic field around the vehicle with different materials: (a) iron, (b) aluminum, and (c) CFRP. © 2019 IEEE

Table 4.1 Comparison between calculated magnetic field strength for WPT systems with a transmitting power of 3.7 kW when the body material of the vehicle is composed of (a) Iron, (b) Aluminum, and (c) CFRP

Position (Figure 2.3)		Calculated magnetic field [A/m]		
		(a)	(b)	(c)
Driver	(A)	0.026	0.026	2.068
	(B)	0.026	0.026	16.34
	(C)	0.058	0.060	4.047
	(G)	0.065	0.060	4.047
Passenger	(D)	0.016	0.017	23.59
	(E)	0.016	0.017	1.382
	(F)	0.047	0.048	1.023

© 2019 IEEE

4.3.2. Induced Electric Field in Human Body

Figure 4.4 (a) and (b) show the distributions of the induced electric field in the human body models as they correspond to the driver and passenger, respectively. When the body material of the vehicle was CFRP, the maximum induced electric field value was 0.52 V/m in the cabin position of (B) (the thigh and buttocks of the model in the driving seat), while it was 0.345 V/m for the model in the rear seat, appearing in the right foot. Both positions of the maximum field strength were close to the WPT system, due to the higher magnetic field strength. When the body material of the vehicle was aluminum and iron, the maximum induced electric field values for the models in the driving seat and rear seat were 0.003 V/m at (C) and (F), corresponding to the trunk and head. The calculated induced electric field is compared to the basic restriction prescribed in the ICNIRP guidelines [2]. Table 4.2 shows the maximum induced electric field value in each body part, along with the basic restriction from the ICNIRP guidelines. Table 4.2 shows that the induced electric fields of all body parts were 0.04 times those of the basic ICNIRP restrictions in Table 1.1.

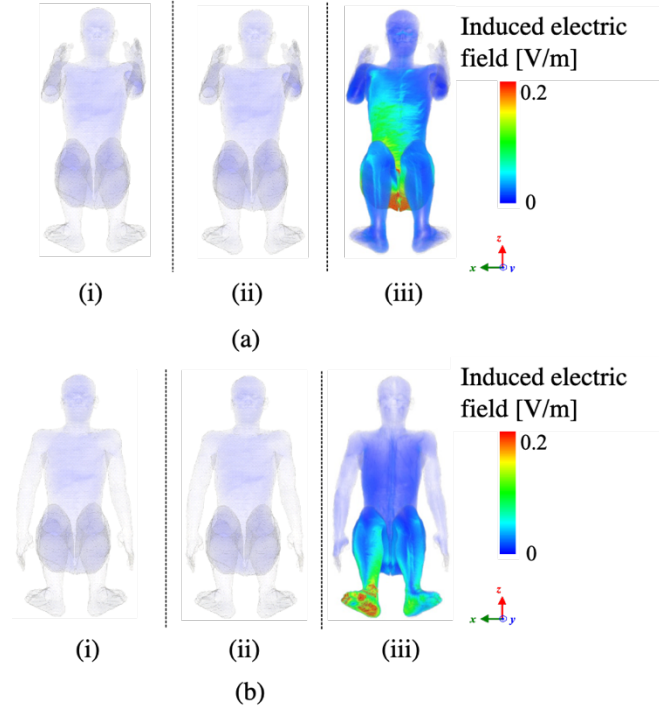


Figure 4.4 Distribution of induced electric field in the models of (a) driver and (b) passenger in the vehicle made of (i) iron, (ii) aluminum, and (iii) CFRP. © 2019 IEEE

Table 4.2 Computed induced electric field value for WPT systems with a transmitting power of 3.7 kW when the body material of the vehicle is composed of (a) Iron, (b) Aluminum, and (c) CFRP.

Position (Figure 2.3)		Calculated induced electric field [V/m]		
		(a)	(b)	(c)
Driver	(A)	0.001	0.001	0.058
	(B)	0.002	0.002	0.525
	(C)	0.003	0.003	0.188
	(G)	0.002	0.002	0.027
Passenger	(D)	0.001	0.001	0.345
	(E)	0.002	0.002	0.074
	(F)	0.003	0.003	0.024

© 2019 IEEE

4.3.3. Coupling Factor

Table 4.3 shows the computed coupling factors for different body parts derived from eq. (2.4). The coupling factors were comparable for aluminum and iron materials, and lower for CFRP. The coupling factors at the shin and arm were lower than at other body parts with different vehicle body materials. According to the obtained coupling factor and eq. (2.4), an empirical estimate of the permissible magnetic field strength can be calculated. For example, using a maximum coupling factor 0.179 at the passenger's thigh and buttocks in Table 4.3 with aluminum or iron vehicle body material, the maximum magnetic field strength in the probe dimension (100 cm^2) was 5.5 times higher than the reference level. Similarly, the permissible magnetic field strength was about 10 times higher than the reference level with a coupling factor of 0.10 for CFRP.

Table 4.3 Value of coupling factor for different body parts when the body material of the vehicle is composed of (a) Iron, (b) Aluminum, and (c) CFRP

Position (Figure 2.3)		Coupling factor		
		(a)	(b)	(c)
Driver	(A)	0.075	0.076	0.051
	(B)	0.129	0.126	0.059
	(C)	0.095	0.094	0.085
	(G)	0.048	0.049	0.045
Passenger	(D)	0.079	0.080	0.027
	(E)	0.172	0.172	0.098
	(F)	0.121	0.117	0.044

© 2019 IEEE

4.4. Discussion & Conclusion

This chapter evaluated the induced electric field in the human body model positioned at the driver and passenger seats of a vehicle body using a WPT system operating at 3.7 kW for local and nonuniform exposure. In particular, different materials were considered for the vehicle body. The coupling factor, which relates the external magnetic field and the induced electric field, was then derived for simple safety assessment of local and nonuniform exposure in vehicle cabins. The main feature of the coupling factor derived in this chapter is that the body is separated into parts for consistency with IEC TS 62764-1. It was also found that when the body material of the vehicle was CFRP, the magnetic field strength leaking into the vehicle was higher than when other materials (iron and aluminum) were used. When the body material of the vehicle was iron or aluminum, the magnetic field leaked from the window into the vehicle interior. The induced electric field strength for CFRP was higher than for other materials. It was confirmed that the induced electric field values were highest at the position where the magnetic fields generated by the WPT system leaked into the vehicle, and that the induced field values of the body parts of both driver and passenger, considered in IEC TS 62764-1, complied with the ICNIRP guidelines [2]. The coupling factors for different body parts were also calculated in this chapter. The coupling factor in the limb (excluding the thigh and buttocks and the trunk) ranged from 0.027 to 0.076, which are comparable to the results of inter-comparison studies on the coupling factor of the human body outside the vehicle cabin [14]. The previous study [14] showed that the coupling factor was less than 0.1 for all cases. The difference from [14] was attributed to the difference in the magnetic field distribution. The induced field is governed by Faraday's law, and thus the field in the leg, where cross-sectional area is smaller than that of the body. Nonuniformity of the field is difficult to generalize, and therefore a conservative (larger) coupling factor would be essential. According to Figure 4.3, the magnetic field strength generated by the WPT leaked directly into the cabin under the floor. The magnetic fields at the case of CFRP has thus more uniformity than that of iron and aluminum where only the diffracted field from windows exists. The coupling factor for CFRP should be higher than that of the iron and aluminum, considering the concept of the coupling factor. However, the coupling factor obtained for CFRP was smaller. The reason for this is that the cross-sectional area of the human body part relative to the magnetic field component. For CFRP the field component perpendicular to the floor is dominant. The projected area of the human body to the vehicle floor is smaller

than that for from the windows. Therefore, the coupling factor for CFRP is smaller than that of iron and aluminum even for higher field uniformity. It was confirmed that when the maximum coupling factor was used in cases with an iron or aluminum vehicle body, the induced electric field was less than the basic restriction described in the ICNIRP guideline, until the magnetic field strength was about 5.9 times higher than the reference level. When the vehicle material was CFRP, the induced electric field was less than the basic restriction until the magnetic field strength was 11.1 times higher than the reference level. This means that a transmitting power of 370 kW is permitted to comply with the ICNIRP guideline. Therefore, the compliance assessment of this scenario became over-conservative, and we need to propose the formula of the induced electric field calculated from the magnetic field strength by use of our proposal in Chapter 3.

In future work, the proposed formula will be applied to nonuniform fields. The future study should be helpful for nonuniform assessment compliance in ICNIRP, IEEE and IEC

Chapter 5

Effects of Skin-to-Skin Contact for Post-processing Algorithm

5.1. Overview

Chapter 3 and 4 employed 99%ile, 99.9%ile value and exclusion of skin-skin contact for post-processing algorithm of the induced electric field. When the induced electric field is computed, segmentation error and the skin-to-skin contact produce locally high electric fields which is not essential to cause the stimulation. We then performed some pre/post-processing which is defined in ICINRP [2] and proposed in previous study[26], [42], [43] to compute the induced electric fields. This Chapter 5 discusses the effects of post-processing of the internal electric field, which is not applied with current crossing skin layers which has been mentioned in the IEEE C95.1

The computational results show that when skin-to-skin contact voxels were excluded, the effect of skin-to-skin contact was also somewhat suppressed and the induced electric field value decrease to from one third to one tenth. However, the coupling factor value of using only 99.9%ile is almost same value as that of using both exclusion of skin-to-skin contact and 99.9%ile. Therefore, we confirmed that the exclusion of skin-to-skin contact which is suggested in the IEEE C95.1- 2019 standard, is not much conservative method in case of considering the different body part in Chapter 3 and 4.

The results presented here were presented in [44].

5.2. Exposure Scenario

The exposure scenario is same as that of Chapter 4. The vehicle model is composed of Iron and CFRP which has different magnetic field distribution according to Figure 4.2 (a) and (c) in Chapter 4. Two positions of realistically postured models are considered: sitting in the driver’s seat and sitting in the passenger’s seat, which is same exposure as Figure 4.1 in Chapter 4.

5.3. Results

5.3.1. Induced Electric Field

This section evaluates the effects of skin-to-skin contact on the induced electric field for a vehicle with iron and CFRP body material. According to IEEE C95.1-2019 standard, dosimetric reference limit (DRLs) do not apply to current crossing skin layers. Figure 5.1 shows the induced electric fields of driver and passenger. As showing in Figure 5.1 (a) and (b), for bodies made of iron and CFRP, this suggests that the voxels with non-negligible computational error may exceed 0.1%ile. Specifically, the effect of skin-to-skin contact was obvious at armpit, the boundary between thigh and buttocks, and that at buttocks for both materials, and passenger’s feet for CFRP. Driver and passenger’s face has also high induced electric field. However, they are not influence of skin-to-skin contact, and attributable to complex structure or the stair-casing error. Therefore, the 99.9%ile for post-processing were also needed. We evaluated the difference with or without exclusion of skin-to-skin contact voxels at passenger’s feet. As shown in Figure 5.2, when skin-to-skin contact voxels were excluded, the influence of skin-to-skin contact between the passenger’s armpit was somewhat suppressed and the induced electric field value

decrease to one tenth (0.74 V/m to 0.08 V/m). In case of driver's thigh and between thigh and buttocks in Figure 5.3 and Figure 5.4 when skin-to-skin contact voxels were excluded, the effects of skin-to-skin contact was also somewhat suppressed and the induced electric field value decrease.

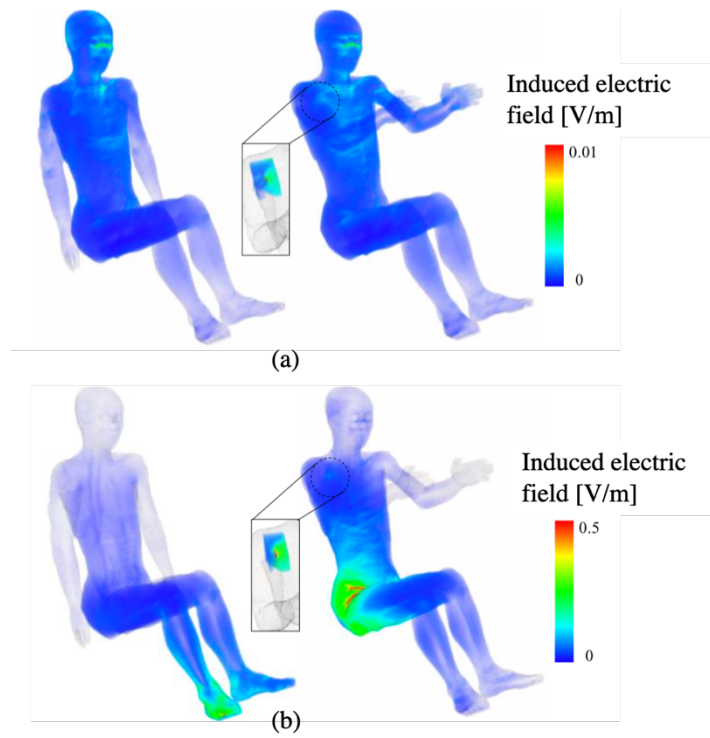


Figure 5.1 Induced electric field in (right) passenger and (left) driver without post-processing: the vehicle body is comprised of (a) iron and (b) CFRP.

© 2020 IEEE

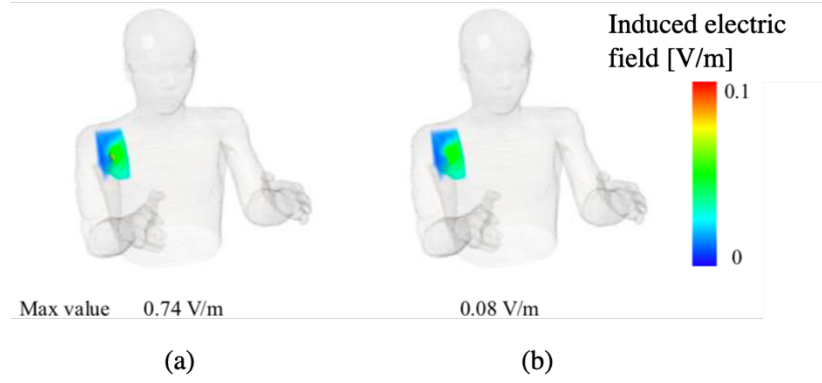


Figure 5.2 Induced electric field of driver's armpit. (a) without post-processing and (b) voxels for skin-to-skin contact is excluded. © 2020 IEEE

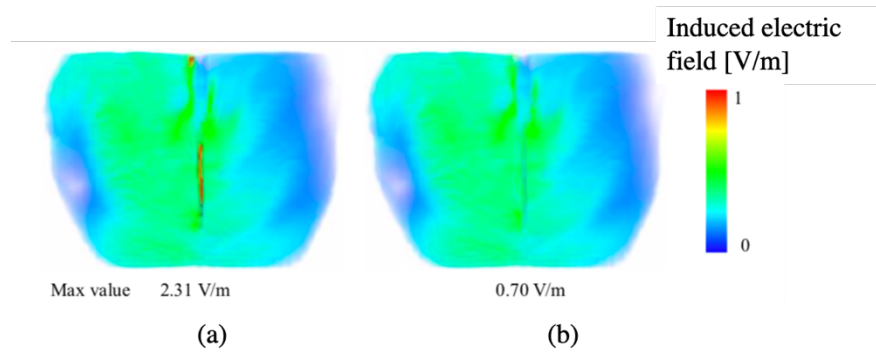


Figure 5.3 Induced electric field of driver's armpit. (a) without post-processing and (b) voxels for skin-to-skin contact is excluded. © 2020 IEEE

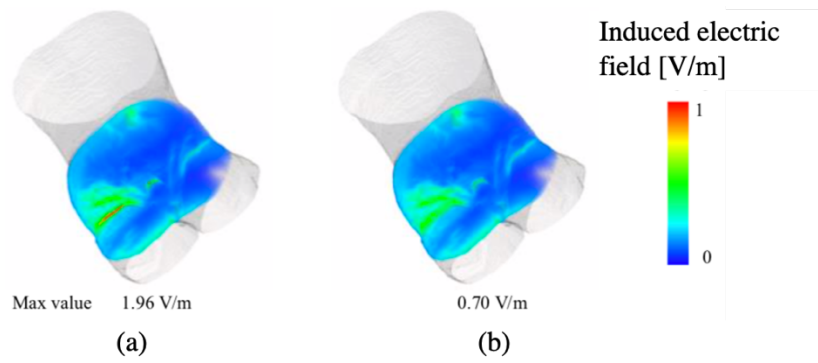


Figure 5.4 Induced electric field of driver's thigh and buttocks. (a) without post-processing and (b) voxels for skin-to-skin contact is excluded. © 2020 IEEE

5.3.2. Coupling Factor

This section evaluates the coupling factor in case of considering skin-to-skin contact or not. The coupling factor is calculated by eq. (2.4). The value of the magnetic field H_{max} in eq. (2.4) used the magnetic field strength in Table 4.1. Table 5.1 shows coupling factors in case of using only 99.9%ile and both exclusion of skin-to-skin contact and 99.9%ile. According to Table 5.1, the coupling factor value of using only 99.9%ile is almost same value as that of using both exclusion of skin-to-skin contact and 99.9%ile. For anatomical human model, which is based on IEC TS 62764, the 99.9%ile of the electric field is enough for different body parts. However, it is also confirmed that the exclusion of skin-to-skin contact is not much different. The values obtained here is consistent with those reported in the intercomparison [14].

Table 5.1 Value of coupling factor for different body parts (a) 99.9%ile and (b) exclusion of skin-to-skin contact and 99.9%ile

Position (Figure 2.3)		Coupling factor	
		(a)	(b)
Driver	(A)	0.051	0.051
	(B)	0.059	0.058
	(C)	0.085	0.085
	(G)	0.048	0.045
Passenger	(D)	0.027	0.027
	(E)	0.098	0.097
	(F)	0.044	0.044

© 2020 IEEE

5.4. Discussion and Conclusion

This chapter evaluated the induced electric field in the human body model positioned at the driver and passenger seats of a vehicle body using a WPT system operating at 3.7 kW, which is same exposure scenario as chapter.4. In particular, the effect of post-processing of the induced electric field which is not applied with current crossing skin layers were considered for each body parts. The computational results show that the influence of skin-to-skin contact causes at armpit, buttocks and between thigh and buttocks of the human body. When skin-to-skin contact voxels were excluded, the effect of skin-to-skin contact was also somewhat suppressed and the induced electric field value decrease to from one third to one tenth. However, the coupling factor value of using only 99.9%ile is almost same value as that of using both exclusion of skin-to-skin contact and 99.9%ile. Therefore, we confirm that the exclusion of skin-to-skin contact which is suggested in the IEEE C95.1-2019 standard, is not much conservative method in case of considering the different body part in Chapter 3 and 4.

Chapter 6

Summary

Studies on human dosimetry and compliance assessment for LF electromagnetic fields recently have attracted attention because of the emergence of wireless technology. In the LF fields exposure (below 100 kHz), electrostimulation caused by an induced electric field in the human body is a dominant factor. In actual scenarios of the human exposure to LF near fields, a limb of the human body is mainly exposed (local exposure). The field distribution is then nonuniform. Therefore, the assessment of local and nonuniform exposure is essential.

Regarding to ICNIRP and IEEE guidelines / standards, the reference level is derived assuming that the human exposed to the uniform field stands in free space. Several studies show that the assessment in terms of the spatial peak field strength may become over-conservativeness because the predicted exposure scenario of the guidelines/ standards may not match that of practical scenarios. The compliance assessment of the basic restriction is thus needed. Regarding to the compliance assessment standards which is published by IEC, although the induced electric field in human body can be calculated at research institutions, compliance assessments for manufacturers should be easier and more practical. Therefore, some compliance assessment standards introduced the coupling factor. However, the method to calculate the coupling factor is not considered in ICNIRP guideline and IEEE standard, and we then should theoretically show the relationship between the magnetic field and the induced electric fields in practical scenarios to help set the permissible external field strength in ICNIRP and IEEE.

First, we proposed a formula in which an induced electric field can be derived in a scenario where the cuboid body part model is exposed to a uniform LF magnetic field for local exposure. When the aspect ratio of the cuboid model as human model is not less than 2:1, the difference in the maximum electric fields obtained from the proposed formula and SPFD was less than 8%,

and that from the FEM results was less than 7%, and we can confirm that the induced electric field can be estimated from the magnetic field strength which flows into the human body. In addition, we compared the induced electric fields in the homogeneous ellipsoidal, homogeneous realistically shaped, and inhomogeneous models for the 99.9%ile value. We also found that the induced electric field in the homogeneous ellipsoidal model defined in IEEE C95.6, was similar to that in the homogeneous model, and the induced electric field in the inhomogeneous model was 1.5 times higher than that of the homogeneous model. These results suggested that the homogeneous ellipsoidal model could be extended for deriving a limit in terms of the induced electric field considering these factors. Thus, a minor revision of the exposure reference level for limbs (partial body) in the IEEE C95.6 standard would provide a more consistent limit. In addition, the ratio will be helpful in deriving the reference level of the ICNIRP guidelines if consistency with the RF guidelines is considered.

Next, we discussed the investigation of the relationship between the external magnetic field, the induced electric field, and the coupling factor for WPT system in local and nonuniform exposure scenario. The WPT system is implemented on a vehicle body which is composed of iron, aluminum, and CFRP. The computational results showed that when the body material of the vehicle was CFRP, the magnetic field strength leaking into the vehicle was higher than when other materials (iron and aluminum) were used. When the body material of the vehicle was iron or aluminum, the magnetic field leaked from the window into the vehicle interior. The magnetic field strength is highest value at passenger's shin when the vehicle body is composed of CFRP, and 1.1 times higher than the reference level of ICNIRP 2010. However, the induced field values of the body parts of passenger complied with the ICNIRP 2010 [2]. Therefore, the compliance assessment of this local and nonuniform scenario became over-conservative. The coupling factor in the limb (excluding the thigh and buttocks and the trunk) ranged from 0.027 to 0.076, The previous study [14] showed that the coupling factor was less than 0.1 for all cases. The difference from [14] was attributed to the difference in the magnetic field distribution. The induced field is governed by Faraday's law, and thus the field in the leg, where cross-sectional area is smaller than that of the body. We then found that nonuniformity of the field is difficult to generalize, and therefore a conservative (larger) coupling factor would be essential.

Finally, we discussed the effects of post-processing of the internal electric field, which is not applied with current crossing skin layers which has been mentioned in the IEEE C95.1 standard-2019. In case of WPT system in practical scenario, the effect of skin-to-skin contact was obvious

at armpit, the boundary between thigh and buttocks, and that at buttocks for both materials, and passenger's feet for CFRP. Driver and passenger's face has also high induced electric field. However, they are not influence of skin-to-skin contact, and attributable to complex structure or the stair-casing error. Therefore, the 99.9%ile for post-processing was also needed. The coupling factor value of using only 99.9%ile is almost same value as that of using both exclusion of skin-to-skin contact and 99.9%ile. Then, we confirmed that the exclusion of skin-to-skin contact which is suggested in the IEEE C95.1- 2019 standard is not much conservative method in case of considering the different body part.

In future work, the proposed formula in Chapter 3 will be applied to nonuniform fields such as human exposure scenario for WPT system. The future study should be helpful for local and nonuniform assessment compliance in ICNIRP, IEEE and IEC The final goal is to bridge the gap between the exposure and product standards, which are discussed separately, as well as to calculate the induced electric field from nonuniform external magnetic field distribution and the size of the human model that is exposed using the proposed formula.

Acknowledgements

Firstly, I would like to express my sincere gratitude to my advisor Prof. Akimasa Hirata for the continuous support of my Ph.D. study and related research, for his patience, motivation, and immense knowledge. His guidance helped me in all the time of research and writing of this thesis.

Besides my advisor, I would like to thank the rest of my thesis committee: Prof. Yoshitsugu Kamimura, Prof. Nobuyoshi Kikuma and Prof. Jianqing Wang for their insightful comments and encouragement, but also for the hard question which incited me to widen my research from various perspectives.

My sincere thanks also go to Dr. Jose Gomez-Tames, Dr. Yinliang Diao, Dr. Junqing Lan, Dr. Sachiko Koderu, Dr. Essam A. Rashed and all of the laboratory member.

Finally, I would like to thank my family for encouraging and supporting the whole process of this research.

References

- [1] ICNIRP, “Guidelines for limiting exposure to time-varying electric, magnetic, and electromagnetic fields (up to 300 GHz),” *Health Phys.*, vol. 74, no. (4), p. 494-522;, 1998.
- [2] ICNIRP, “Guidelines for limiting exposure to time-varying electric and magnetic fields (1 Hz to 100 kHz),” *Health Phys.*, vol. 99, no. 6, pp. 818–836, 2010.
- [3] *IEEE Standard for Safety Levels With Respect to Human Exposure to Radio Frequency Electromagnetic Fields, 3 kHz to 300 GHz*, IEEE Standard C95.1, 2006.
- [4] *IEEE Standard for Safety Levels With Respect to Human Exposure to Electric, Magnetic and Electromagnetic Fields, 0 Hz to 300 GHz*, IEEE Standard C95.1, 2019.
- [5] *IEEE Standard for Safety Levels With Respect to Human Exposure to Electromagnetic Fields, 0 to 3 KHz*, IEEE Standard C95.6, 2002.
- [6] IEC 62233, “Measurement methods for electromagnetic fields of household appliances and similar apparatus with regard to human exposure,” 2005.
- [7] IEC 62226-2-1, “Exposure to electric or magnetic fields in low and intermediate frequency range – Methods for calculating the current density and induced electric field induced in the human body,” 2004.
- [8] IEC PAS 63184 ED1, “Assessment methods of the human exposure to electric and magnetic fields from wireless power transfer systems - Models, instrumentation, measurement and numerical methods and procedures (frequency range of 1 kHz to 30 MHz),” 2021.
- [9] S. Schottke, J. Meyer, P. Schegner, and S. Bachmann, “Emission in the frequency range of 2 kHz to 150 kHz caused by electrical vehicle charging,” in *Proc. Int. Symp. Electromagn. Compat.*, 2014, pp. 620–625.
- [10] A. Khaligh and S. Dusmez, “Comprehensive topological analysis of conductive and inductive charging solutions for plug-in electric vehicles,” *IEEE Trans. Veh. Technol.*, vol. 61, no. 8, p. 3475, 2012.
- [11] IEC TS 62764-1, “Measurement procedures of magnetic field levels generated by electronic and electrical equipment in the automotive environment with respect to human exposure - Part 1: Low frequency magnetic fields,” 2019.
- [12] I. Laakso and A. Hirata, “Evaluation of the induced electric field and compliance procedure for a wireless power transfer system in an electrical vehicle,” *Phys. Med. Biol.*, vol. 58, no. 21, pp. 7583–7593, Nov. 2013.
- [13] X. L. Chen *et al.*, “Human exposure to close-range resonant wireless power transfer systems as a function of design parameters,” *IEEE Trans. Electromagn. Compat.*, vol. 56, no. 5, pp. 1027–1034, Oct. 2014.

- [14] K. Wake *et al.*, “Derivation of coupling factors for different wireless power transfer systems: Inter- and intralaboratory comparison,” *IEEE Trans. Electromagn. Compat.*, vol. 59, no. 2, pp. 677–685, Apr. 2017.
- [15] T. Sunohara, A. Hirata, I. Laakso, V. de Santis, and T. Onishi, “Evaluation of nonuniform field exposures with coupling factors,” *Phys. Med. Biol.*, vol. 60, no. 20, pp. 8129–8140, 2015.
- [16] Y. Hakuta, T. Watanabe, T. Takenaka, T. Ito, and A. Hirata, “Safety Standard Compliance of Human Exposure From Vehicle Cables Using Coupling Factors in the Frequency Range of 0.3–400 kHz,” *IEEE Trans. Electromagn. Compat.*, pp. 1–6, 2020.
- [17] T. Shimamoto, I. Laakso, and A. Hirata, “In-situ electric field in human body model in different postures for wireless power transfer system in an electrical vehicle,” *Phys. Med. Biol.*, vol. 60, no. 1, pp. 163–173, 2015.
- [18] A. Hirata, K. Caputa, T. W. Dawson, and M. A. Stuchly, “Dosimetry in models of child and adult for low-frequency electric field,” *IEEE Trans. Biomed. Eng.*, vol. 48, no. 9, pp. 1007–1012, Sep. 2001.
- [19] T. W. Dawson and M. A. Stuchly, “High-resolution organ dosimetry for human exposure to low-frequency magnetic fields,” *IEEE Trans. Magn.*, vol. 34, no. 3, pp. 708–718, May 1998.
- [20] J. Lin, M. Lu, T. Wu, L. Yang, and T. Wu, “Evaluating extremely low frequency magnetic fields in the rear seats of the electric vehicles,” *Radiat. Protection Dosimetry*, vol. 182, no. 2, pp. 190–199, 2018.
- [21] K. Yamazaki, M. Taki, and C. Ohkubo, “Safety assessment of human exposure to intermediate frequency electromagnetic fields,” *Elect. Eng. Jpn.*, vol. 197, no. 4, pp. 3–11, 2016.
- [22] B. Kos, B. Valic, T. Kotnik, and P. Gajsek, “Induced electric fields in workers near low-frequency induction heating machines,” *Bioelectromagnetics*, vol. 35, no. 3, pp. 222–226, 2014.
- [23] Y. L. Diao, W. N. Sun, Y. Q. He, S. W. Leung, and Y. M. Siu, “Equivalent magnetic vector potential model for low-frequency magnetic exposure assessment,” *Phys. Med. Biol.*, vol. 62, no. 19, pp. 7905–7922, 2017.
- [24] T. Shimamoto, I. Laakso, and A. Hirata, “Internal electric field in pregnant- woman model for wireless power transfer systems in electric vehicles,” *Electron. Lett.*, vol. 51, pp. 2136–2137, 2015.
- [25] B. Kos, B. Valič, D. Miklavčič, T. Kotnik, and P. Gajšek, “Pre- and post-natal exposure of children to EMF generated by domestic induction cookers,” *Phys. Med. Biol.*, vol. 56, no. 19, pp. 6149–6160, Oct. 2011.
- [26] J. Gomez-Tames, I. Laakso, Y. Haba, A. Hirata, D. Poljak; K. Yamazaki, “Computational Artifacts of the In Situ Electric Field in Anatomical Models Exposed to Low-Frequency Magnetic Field,” *IEEE Trans. Electromagn. Compat.*, pp. 589–597, 2018.
- [27] V. de Santis, X. L. Chen, I. Laakso, and A. Hirata, “An equivalent skin conductivity model for low-frequency magnetic field dosimetry,” *Biomed. Phys. Eng. Express*, vol. 1, no. 1, 2015.

- [28] A. Hirata, F. Ito, and I. Laakso, "Confirmation of quasi-static approximation in SAR evaluation for a wireless power transfer system," *Phys. Med. Biol.*, vol. 58, no. 17, pp. N241–N249, Sep. 2013.
- [29] S. Gabriel, R. W. Lau, and C. Gabriel, "The dielectric properties of biological tissues: II. Measurements in the frequency range 10 Hz to 20 GHz," *Phys. Med. Biol.*, vol. 41, no. 11, pp. 2251–2269, 1996.
- [30] SAE J2954, "Wireless Power Transfer for Light-Duty Plug-In/Electric Vehicles and Alignment Methodology," 2016. .
- [31] V. de Santis, T. Campi, S. Cruciani, I. Laakso, and M. Feliziani, "Assessment of the induced electric fields in a carbon-fiber electrical vehicle equipped with a wireless power transfer system," *Energies*, vol. 11, no. 3, 2018, Art. no. 684.
- [32] A. Yao, S. Odawara, and K. Fujisaki, "Iron loss and hysteretic properties under PWM inverter excitation at high ambient temperature," *IEEE J. Ind.*, vol. 7, no. 4, pp. 298–304, 2018.
- [33] Y. Hori and Y. Yokoi, "*Wireless Power Transfer and Infrastructure Construction for Electric Vehicle(Popular Edition)*," 2011.
- [34] T. W. Dawson and M. A. Stuchly, "Analytic validation of a three-dimensional scalar-potential finite-difference code for low-frequency magnetic induction," *Appl. Comput. Electromagn. Soc. J.*, vol. 11, no. 3, pp. 72–81, 1996.
- [35] I. Laakso, and A. Hirata, "Fastmultigrid-basedcomputationoftheinduced electric field for transcranial magnetic stimulation," *Phys. Med. Biol.*, vol. 57, no. 23, pp. 7753–7765, 2012.
- [36] Roger W. Pryor, *Multiphysics Modeling Using COMSOL*. 2009.
- [37] E. A. Rashed, D. Yinliang, T. Shota, T. Sakai, J. Gomez-Tames, and A. Hirata, "Effect of Skin-to-Skin Contact on Stimulation Threshold and Dosimetry," *IEEE Trans. Electromagn. Compat.*, vol. 62, no. 6, pp. 2704–2713, Dec. 2020.
- [38] K. Miwa, Y. Suzuki, J. Lan, Y. Diao and A. Hirata, "A Novel Method to Predict the Maximum Electric Fields in Different Body Parts Exposed to Uniform Low-Frequency Magnetic Field," in *IEEE Transactions on Electromagnetic Compatibility*, vol. 63, no. 5, pp. 1640-1648, Oct. 2021..
- [39] K. Miwa, T. Takenaka, and A. Hirata, "Electromagnetic Dosimetry and Compliance for Wireless Power Transfer Systems in Vehicles," *IEEE Trans. Electromagn. Compat.*, vol. 61, no. 6, pp. 2024–2030, 2019.
- [40] K. Taguchi, "Relationship of external field strength with local and whole-body averaged specific absorption rates in anatomical human models," *IEEE Access*, vol. 6, pp. 70186–70196, 2018.
- [41] B. R. McLeod, A. A. Pilla, and M. W. Samsel, "Electromagnetic fields induced by Helmholtz aiding coils inside saline-filled boundaries," *Bio- electromagnetics*, vol. 4, pp. 357–370, 1983.

- [42] J. F. Bakker *et al.*, “Children and adults exposed to low-frequency magnetic fields at the ICNIRP reference levels: Theoretical assessment of the induced electric fields,” *Phys. Med. Biol.*, vol. 57, no. 7, pp. 1815–1829, 2012.
- [43] I. Laakso and A. Hirata, “Reducing the staircasing error in computational dosimetry of low-frequency electromagnetic fields,” *Phys. Med. Biol.*, vol. 57, no. 4, pp. N25–N34, Feb. 2012.
- [44] K. Miwa, T. Takenaka, and A. Hirata, “Dosimetry and Compliance for Wireless Power Transfer Systems in Vehicle,” *EMC Europe*, Sept. 2020, pp. 1-4, DOI: 10.1109/EMCEUROPE48519.2020.924584

Publication Lists

Peer Reviewed Journal Papers for Thesis

- i. K. Miwa, T. Takenaka and A. Hirata, “Electromagnetic Dosimetry and Compliance for Wireless Power Transfer Systems in Vehicles,” IEEE Transactions on Electromagnetic Compatibility, vol. 61, no. 6, pp.2024-2030, Dec. 2019.
- ii. K. Miwa, Y. Suzuki, J. Lan, Y. Diao, and A. Hirata, “A Novel Method to Predict the Maximum Electric Fields in Different Body Parts Exposed to Uniform Low-Frequency Magnetic Field,” IEEE Transactions on Electromagnetic Compatibility, Vol. 63, no. 5 pp1640-1648, Oct. 2021.

Peer Reviewed Journal Paper

- iii. J. Gomez-Tames, T. Tarnaud, K. Miwa, A. Hirata, T. Van de Steene, L. Martens, E. Tanghe and W. Joseph, “Brain Cortical Stimulation Thresholds to Different Magnetic Field Source Exposure at Intermediate Frequency,” IEEE Transactions on Electromagnetic Compatibility, Vol. 61, pp.1944-1952, Dec. 2019

Peer Reviewed Conference Proceeding Paper for Thesis

- iv. K. Miwa, T. Takenaka, A. Hirata, “Dosimetry and Compliance for Wireless Power Transfer Systems in Vehicle,” EMC Europe, Sept. 2020, pp. 1-4, DOI: 10.1109/EMCEUROPE48519.2020.9245849

Conference Presentations

- v. K. Miwa, “Human Dosimetry and Compliance for Wireless Power Transfer Systems in Vehicle,” IEEE MTT-S Nagoya Chapter Workshop on Human Safety from Electromagnetic Fields, Nov. 2020.

- vi. K. Miwa, Y. Suzuki, Y. Diao. A. Hirata, “In situ Electric Field in Different Body Parts for Exposure to Uniform Magnetic Field,” IEEE International Committee on Electromagnetic Safety TC95 SC6 Meeting, Jun. 2020
- vii. K. Miwa, Y. Suzuki, Y. Diao. A. Hirata, “In situ Electric Field in Different Body Parts For Exposure to Non-Uniform Magnetic Field,” IEEE International Committee on Electromagnetic Safety TC95 SC6 Meeting Jan. 2021